Rational design and molecular engineering of ultrastable porous fluorescent guanidine functionalized polybenzoxazine

Mohammed G. Kotp [a], Mohamed Gamal Mohamed [a,b], Aya Osama Mousa [a], Shiao-Wei Kuo [a,c,*]

[a] Department of Materials and Optoelectronic Science, Center for Functional Polymers and Supramolecular Materials, National Sun Yat-Sen University, Kaohsiung 804, Taiwan
[b] Chemistry Department, Faculty of Science, Assiut University, Assiut 71515, Egypt
[c] Department of Medicinal and Applied Chemistry, Kaohsiung Medical University, Kaohsiung 807, Taiwan

ABSTRACT

This study reports the design, synthesis, and characterization of a novel compound, 1,2,3-tris(7-bromo-2H-benzo [e][1,3]oxazin-3(4H)-yl)guanidine (BGu-BZ), using triaminoguanidinium chloride (Gu-3NH$_2$) as a precursor through a straightforward Mannich condensation reaction. The resulting benzoxazine monomer exhibited distinct fluorescence properties influenced by solvent polarity, with emission maxima shifting across solvents. Thermal curing of BGu-BZ at 220 °C yielded poly(BGu-BZ), a porous polymer with enhanced fluorescence emission and excellent thermal stability (T$_{d10}$ = 381.5 °C). The cured polymer demonstrated a surface area of 43 m^2/g and significant fluorescence shifts, confirming alterations in electronic structure and increased conjugation. The study highlights the solvatochromism behavior of both monomer and polymer, underscoring their potential for applications in luminescent technologies such as solvent sensing and optoelectronics. This work provides valuable insights into the structural-functional relationship in guanidine-functionalized benzoxazines, paving the way for advanced material applications.

1. Introduction

Benzoxazines (BZs) are a class of heterocyclic compounds that have attracted considerable interest in materials science due to their unique chemical properties and broad range of applications [1–3]. Characterized by a six-membered oxazine ring containing nitrogen and oxygen, these compounds are typically synthesized from phenolic derivatives, formaldehyde, and primary amines [4,5]. Polybenzoxazines (PBZs), the polymerized form of benzoxazines, exhibit exceptional thermal stability, mechanical strength, and low shrinkage during curing, making them attractive alternatives to traditional thermosetting resins such as phenolics and epoxies [6,7]. Their remarkable thermal stability is largely attributed to the robust intermolecular and intramolecular hydrogen bonding within their structure, enabling superior performance in high-temperature applications [8–11]. One of the defining advantages of benzoxazines is their versatility, as the incorporation of various functional groups into PBZs enhances their adhesion properties and overall durability [12–14]. This adaptability has expanded their utility across multiple industries. In particular, PBZs have found increasing

application in advanced coatings, such as anti-corrosion and self-cleaning surfaces [15,16]. Their ability to form strong bonds with substrates significantly improves the longevity and effectiveness of these protective coatings. Given their advantageous properties, benzoxazines are playing an increasingly prominent role in modern materials science, offering innovative solutions for high-performance applications [17].

Recent research has explored the integration of benzoxazines into luminescent compounds, broadening their application in optoelectronic devices and sensors [18]. Innovations in benzoxazine chemistry have also paved the way for the development of smart materials with self-healing capabilities, shape-memory effects, and dynamic responsiveness to environmental stimuli [18–22]. Ongoing studies continue to focus on the functionalization and modification of benzoxazines to further enhance their performance and expand their applicability in advanced materials science.

Triaminoguanidinium chloride (Gu-3NH$_2$) plays a crucial role as a precursor in synthesizing innovative porous derivatives, particularly for advanced polymeric materials [23]. Its unique structural features significantly enhance the properties of the resulting polymers [24]. The

* Corresponding author at: Department of Materials and Optoelectronic Science, Center for Functional Polymers and Supramolecular Materials, National Sun Yat-Sen University, Kaohsiung 804, Taiwan.
E-mail address: kuosw@faculty.nsysu.edu.tw (S.-W. Kuo).

threefold symmetry of Gu-3NH$_2$ facilitates the incorporation of diverse functional groups, enabling precise tailoring of the chemical and physical characteristics of the final products [25]. The amino groups in Gu-3NH$_2$ offer additional benefits by participating in hydrogen bonding interactions within the polymer matrix [26]. These interactions improve the thermal stability of guanidinium benzoxazine derivatives and contribute to maintaining structural integrity under varying environmental conditions [27]. The ability to form stable hydrogen bonds not only enhances thermal properties but also ensures the robustness of the material in demanding applications. Beyond its structural advantages, Gu-3NH$_2$ is expected to serve as a versatile platform for synthesizing benzoxazine derivatives with desirable optical properties [28]. Incorporating triaminoguanidinium into benzoxazine frameworks can improve fluorescence characteristics, making these materials highly suitable for optoelectronic and sensing technologies. However, despite these promising possibilities, guanidinium benzoxazine derivatives' characteristics and photophysical behavior remain largely unexplored. This gap presents exciting opportunities for further research to unlock the full potential of these innovative materials. Our work suggests a straightforward thermal curing process, setting it apart from prior studies reliant on pyrolysis or limited to antibacterial, adsorption, or chiral optical properties [29–31] Unlike former studies, which focus on conventional benzoxazines or their nanocomposites, the current provides the first detailed investigation into the solvatochromism behavior of guanidine-functionalized benzoxazines, offering insights into their fluorescence shifts in response to solvent polarity. This property opens pathways for sensing and optoelectronic applications, which are not commonly addressed in prior works.

In this study, we designed an innovative benzoxazine monomer, BGu-BZ, through a three-step synthesis process [Fig. 1]. The structural integrity of BGu-BZ was thoroughly confirmed using advanced characterization techniques, including Fourier-transform infrared spectroscopy (FTIR). Following the successful synthesis of BGu-BZ, thermal curing at 220 °C was performed to produce the derived poly(BGu-BZ), which exhibited a surface area of 43 m^2/g and demonstrated excellent thermal stability. Furthermore, the fluorescence emission properties of both the pristine BGu-BZ and the poly(BGu-BZ) were characterized across various solvents. The results revealed significant sensitivity of fluorescence behavior to solvent polarity and curing effects, providing valuable insights into the optical properties of these materials.

2. Experimental Section

2.1. Materials

The materials utilized in the current research include guanidine hydrochloride, hydrazine monohydrate (NH$_2$NH$_2$·H$_2$O), paraformaldehyde [(CH$_2$O)$_n$], 1,4-dioxane (DO), 4-bromo-2-hydroxybenzaldehyde, ethanol (EtOH), and sodium borohydride (NaBH$_4$) were used as received without any further purification.

2.2. Synthesis of triaminoguanidinium chloride (Gu-3NH$_2$)

Firstly, Gu-3NH$_2$ was synthesized using the following procedure as reported before [32]. Initially, 1.9 g (19.9 mmol) of guanidine hydrochloride was combined with 3.4 g (68 mmol) of NH$_2$NH$_2$·H$_2$O in 10 mL of DO. This mixture was subjected to reflux for four hours under a nitrogen atmosphere. After the reaction, the mixture was allowed to cool to room temperature, and the resulting white solid was filtered out and thoroughly washed with an additional DO to remove any excess NH$_2$NH$_2$·H$_2$O. The solid product was then dried under vacuum at 70 °C, achieving a yield of 99 %. The characterization of Gu-3NH$_2$ was confirmed by comparing its FTIR spectrum [**Fig. S1**] with previously published data, revealing significant peaks at 3331, 3205, 1675, 1599, and 1125 cm^{-1}. ^{13}C NMR (DMSO-$_{d6}$, ppm, [**Fig. S2**]): 157.86 (C = N).
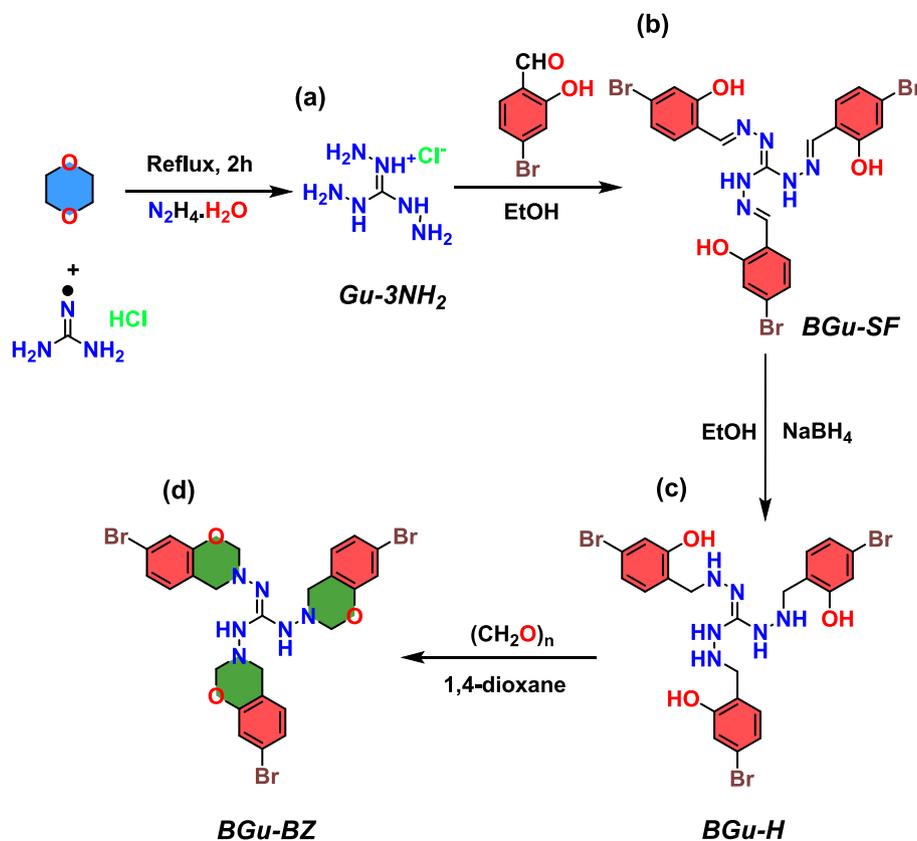

Fig. 1. Synthesis of the BGu-BZ from Gu-3NH$_2$ through the classical multiple-step protocol.

2.3. Synthesis of N',N'',2-tris((E)-4-bromo-2-hydroxybenzylidene) hydrazine-1-carbohydrazonhydrazide (BGu-SF)

A solution containing 5.00 g (35 mmol) of Gu-3NH$_2$ and 2.38 g (11 mmol) of 4-bromo-2-hydroxybenzaldehyde was prepared in 300 mL of EtOH and refluxed overnight at 90 °C. Following the reaction, a white-yellow solid was obtained, which was washed with ethanol, collected, and dried overnight at 60 °C, resulting in a yield of 88 %. The characterization of the product included FTIR analysis showed signals at 3352, 3250, 3066, 1648, and 1609 cm^{-1}. Additionally, the ^{1}H NMR spectrum in DMSO-d_6 revealed chemical shifts at $\delta = 8.98$ ppm (OH), 8.15 ppm (N = CH), and a range from 7.20 to 7.11 ppm for the aromatic protons [**Fig. S3**]. The ^{13}C NMR spectrum in DMSO-d_6 displayed signals at $\delta = 160.59$ ppm for C-OH, as well band at 157.77 ppm for N = CH and a range from 149.01 to 118.96 ppm for the aryl carbon nuclei [**Fig. S4**].

2.4. Synthesis of N',N'',2-tris(4-bromo-2-hydroxybenzyl)hydrazine-1-carbohydrazonhydrazide (BGu-H)

In an ice bath, a mixture of the earlier designed BGu-SF (2.5 g, 3.82 mmol), NaBH$_4$ (1.13 g, 29.87 mmol), and 60 mL of EtOH was mixed and then continuously stirred for 24 h at 25 °C. After this period, the mixture was poured into ice water. The resulting yellow solid was filtered, washed three times with water, and then dried, yielding 95 %. The product was characterized using FTIR (KBr), which displayed absorption peaks at 3400, 3026, 1712, and 1623 cm^{-1}.

2.5. Synthesis of BGu-BZ

A mixture consisting of BGu-H (1.00 g, 1.44 mmol), (CH$_2$O)$_n$ (0.425 g, 14.15 mmol), and a solvent mixture of EtOH/DO (1:2, 30 mL) was heated for 24 h at 110 °C under a nitrogen atmosphere. After heating, the solvent was removed using a rotary evaporator. The remaining residue was treated with hexane and then placed in a refrigerator for 24 h. The resulting bright yellow solid was filtered, washed three times with EtOH, and dried, yielding 75 %. Characterization of the product included FTIR analysis which showed absorption peaks at 3465, 3014, 1635, 1287, and 943 cm^{-1}. Additionally, the ^{1}H NMR spectrum in DMSO-d_6 revealed chemical shifts at 7.12, 6.99, and 6.96 ppm for the aromatic protons, at $\delta = 5.74$ ppm and 4.58 ppm revealed for those protons incorporated oxazine rings [**Fig. S5**]. The ^{13}C NMR spectrum in DMSO-d_6 displayed signals at δ a range from 190.1 (C = N), 156.7 (C-Br), 156.22 to 118.28 ppm for the aryl carbon nuclei, $\delta = 144.41$ ppm for the C core of the guanidinium unit. Moreover, the $\delta = 82.12$ ppm and 56.04 ppm reveal to those carbons of the oxazine units [**Fig. S6**].

2.6. BGu-BZ derived porous polymer [poly(BGu-BZ)]

Poly(BGu-BZ) was synthesized through the ring-opening polymerization of the BGu-BZ at various temperatures: 120, 150, 180, and 220 °C. The curring and polymerization process was carried out for 2 h at each specified temperature.

3. Results and Discussion

3.1. Synthesis, characterization and thermal curing polymerization of BGu-BZ

The synthesis of Gu-3NH$_2$ was achieved by reacting guanidine hydrochloride with hydrazine hydrate in DO, which functioned as both solvent and catalyst. This compound served as a precursor for the preparation of BGu-BZ through a classical multistep synthetic pathway. In the first step, Gu-3NH$_2$ was reacted with 4-bromo-2-hydroxybenzaldehyde to form an intermediate compound, designated as BGu-SF. The intermediate BGu-SF was subsequently reduced to BGu-H using sodium borohydride at room temperature. Finally, a Mannich reaction was

performed by treating the reduced compound with paraformaldehyde in EtOH/DO ethanol at 110 °C, forming BGu-BZ, which precipitated as a yellow solid (Fig. 1). **Fig. S1** presents the FTIR spectrum of Gu-3NH$_2$, highlighting key functional group vibrations. A prominent peak at 3331 cm^{-1} corresponds to the N–H antisymmetric stretching mode, while a symmetric stretching mode of another NH bond is observed at 3302 cm^{-1}. Additional bands at 1675 cm^{-1} and 1599 cm^{-1} are attributed to the stretching vibrations of aromatic C = N and C = C bonds, respectively. Furthermore, the spectrum displays a C–N bond stretching band for the tertiary amine at 1125 cm^{-1}, collectively confirming the molecular characteristics of Gu-3NH$_2$ [33]. The FTIR spectrum of the intermediate compound BGu-SF (Fig. 2) shows key absorption bands at 3066 cm^{-1} and 1648 cm^{-1}. The band at 3066 cm^{-1} corresponds to aryl C–H stretching vibrations, indicating the aromatic nature of the compound. The 1648 cm^{-1} band is attributed to C = N bond stretching vibrations, confirming the presence of imine functionality. Additionally, aromatic C = C bond stretching vibrations are observed at 1609 cm^{-1}, further supporting the aromatic character of BGu-SF. In contrast, the FTIR spectrum of BGu-H reveals a broad absorption band around 3400 cm^{-1}, attributed to O–H and N–H stretching vibrations. This broad peak suggests intermolecular hydrogen bonding, which is characteristic of compounds with hydroxyl and amine groups. An absorption band at 3026 cm^{-1} corresponds to aryl C–H stretching vibrations, reaffirming the compound's aromatic nature. Notably, distinct bands at 1712 cm^{-1} and 1623 cm^{-1} are assigned to stretching vibrations of aromatic C = N and C = C bonds, respectively. These changes in the spectrum reflect modifications in the electronic environment due to the reduction of BGu-SF to BGu-H, confirming successful transformation. The FTIR spectrum of the final product, BGu-BZ, exhibits characteristic peaks crucial for structural confirmation. A peak at 3465 cm^{-1} corresponds to N–H stretching vibrations, indicating the presence of amine groups. The absorption band at 3014 cm^{-1} is assigned to aryl C–H stretching vibrations, confirming aromatic character. A peak at 1635 cm^{-1} signifies aromatic C = C bond stretching. Notably, bands at 1247 cm^{-1} and 943 cm^{-1} are attributed to oxazine rings, hallmark features of benzoxazine compounds. Conversely, the ^{13}CNMR spectrum for BGu-BZ (**Fig. S5**) displays a peak at 144.41 ppm associated with the core C–N part of the guanidinium monomer, confirming its structural features. Additionally, a similar signal pattern is observed within the range of 156.22 to 118.28 ppm, corresponding to aryl carbons in BGu-Bz. Notably, peaks indicating carbons from the oxazine ring appear at 82.12 ppm for OCH$_2$N and 56.04 ppm for ArCH$_2$N, thereby confirming the incorporation of oxazine moieties into the BGu-Bz structure. All these distinct spectral features validate the structural identity of BGu-BZ as a benzoxazine
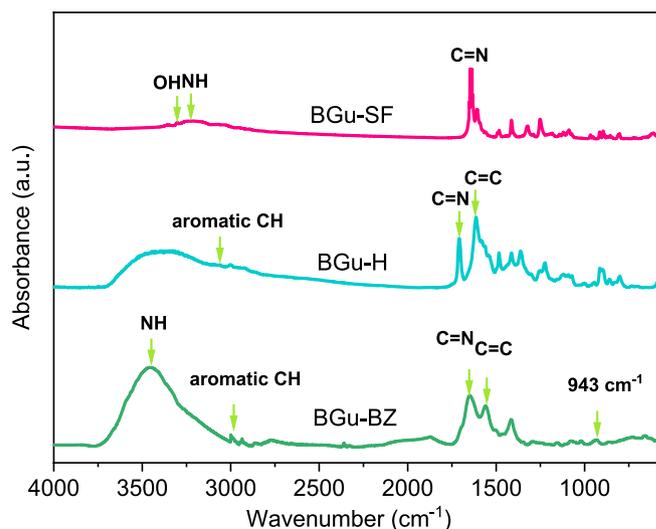

Fig. 2. FTIR scans of BGu-SF, BGu-H, and BGu-BZ.

derivative. The thermal behavior of the BGu-BZ monomer was investigated using DSC under a nitrogen atmosphere, following thermal curing at various temperatures ranging from 120 to 220 °C with a heating rate of 20 °C per minute. The DSC thermograms [Fig. 3(a)] revealed that the uncured BGu-BZ monomer exhibited a prominent exothermic peak at a maximum temperature of 199 °C, with the heat of polymerization measured at 139.7 J g^{-1}. This exothermic peak marks the onset of polymerization, reflecting the energy released during the curing process. As the curing temperature increased, the enthalpy values associated with these exothermic reactions gradually decreased. Notably, exothermic peaks were observed at 205 °C, 207 °C, and 207 °C for curing temperatures of 120 °C, 150 °C, and 180 °C, respectively. The corresponding reaction heats were quantified as 91.52 J g^{-1}, 87.79 J g^{-1}, and 79.51 J g^{-1}. This progressive reduction in heat values indicates a decline in available reactive sites as polymerization advances, suggesting that the system approaches saturation as the curing process nears completion. While the majority of the polymerization is achieved by 220 °C, this minor peak suggests that complete curing may necessitate slightly higher temperatures or prolonged heating [Fig. 3(a)]. On the other hand, such presence of a couple of exothermic peaks during the DSC heating tracks is attributed to the stepwise curing mechanism of BGu-BZ. The first exothermic peak (observed around 199 °C) corresponds to the ring-opening polymerization of the oxazine rings, which forms the initial polymer network. The second, broader exothermic peak (appearing at higher temperatures) is likely to be due to post-curing reactions, such as cross-linking or rearrangement of residual reactive groups. These secondary reactions enhance the network's cross-linking density, improving the thermal stability of the final polymer [4]. Notably, such phenolic hydroxyl-containing byproducts from the Mannich reaction can catalyze the ring-opening polymerization of benzoxazine, leading to a lower curing temperature. The observed lower initial curing temperature of BGu-BZ compared to standard benzoxazine monomers could indeed be influenced by such byproducts. These findings provide valuable insights into the curing behavior and optimal conditions for achieving a stable polymer network. The FTIR spectrum of the uncured BGu-BZ monomer reveals a characteristic peak at 1247 cm^{-1}, corresponding to the asymmetric stretching of the C–O–C bond in the benzoxazine structure, and another peak at 943 cm^{-1}, attributed to the oxazine ring (Fig. 2). These peaks confirm the presence of intact benzoxazine rings in the monomer before curing. As the curing temperature increases from 120 °C to 180 °C, a gradual decline in the intensity of these peaks is observed, indicating the progression of the ring-opening polymerization process. This reduction in peak intensity reflects
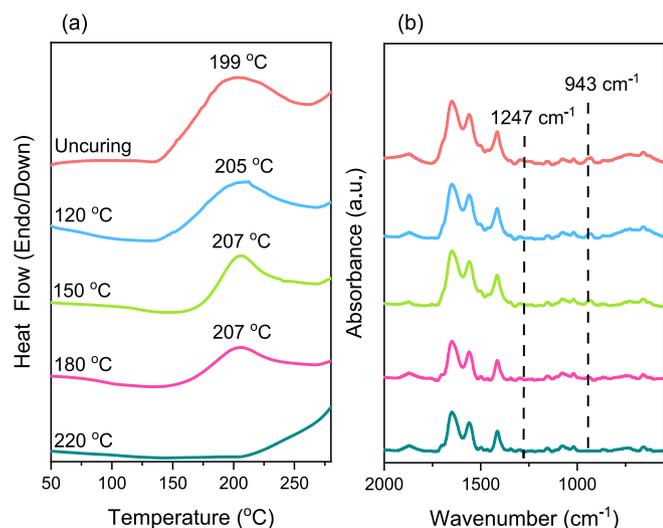
the decreasing concentration of unreacted monomers and the increasing formation of polymerized material [Fig. 3(b)]. At temperatures above 220 °C, the characteristic peaks associated with the oxazine ring and C–O–C stretching completely vanish from the spectrum [Fig. 3(b)]. This disappearance signifies the completion of the thermal polymerization process, resulting in a fully cured polymer devoid of any remaining benzoxazine functionality. The absence of these peaks confirms that all reactive sites have participated in cross-linking reactions, yielding a stable and robust polymeric network. These findings provide valuable insights into the thermal behavior and polymerization characteristics of BGu-BZ. The progressive decline of specific FTIR absorption peaks with increasing curing temperature underscores the dynamic nature of the ring-opening process, which is critical for tailoring material properties. The complete disappearance of these peaks at elevated temperatures validates successful polymerization and highlights the stability of the resulting polymer. The glass transition temperature (T_g) of poly(BGu-BZ) was determined to be 234 °C after thermal curing at 220 °C as shown in **Fig. S7**. This T_g is significantly higher than those typically observed in conventional polybenzoxazine polymers, reflecting the enhanced thermal stability and rigidity of the material [34–42]. The thermal polymerization characteristics of BGu-BZ were further studied using DSC profiles recorded at different heating rates of 20, 15, 10, and 5 °C/min [**Fig. S8**]. The analysis revealed a systematic shift in the exothermic peak temperatures, which occurred at 203 °C, 199 °C, 191 °C, and 185 °C, respectively. This trend indicates that as the heating rate decreases, the maximum exothermic reaction temperature also decreases. This shift can be explained by the effect of the heating rate on the polymerization kinetics. At higher heating rates, the sample has less time to achieve thermal equilibration, leading to higher exothermic peak temperatures as the material reacts more rapidly upon reaching the critical temperature. Conversely, at lower heating rates, the system has more time to equilibrate, allowing reactions to occur at lower temperatures. This behavior aligns with established thermal kinetics principles, where reaction rates are influenced by both temperature and the applied heating conditions [43,44]. These findings provide a deeper understanding of the polymerization dynamics of BGu-BZ, offering insights into optimizing its processing parameters. To determine the activation energy (E_a) associated with the thermal polymerization of BGu-Bz, the Kissinger and Ozawa models were applied to the DSC data (Fig. 4) [45]. The activation energies calculated using these models were 128.20 kJ/mol and 133.75 kJ/mol, respectively. The Kissinger method is a widely used approach for estimating activation energy from DSC data. It analyzes the relationship between the heating rate and peak temperature by plotting $\ln(\beta/T_p^2)$ versus $1/T_p$ [46], where the slope of the resulting straight line is proportional to E_a. This method assumes first-order

Fig. 3. DSC profiles (a) and FTIR scans (b) of BGu-BZ which cured at a series of temperatures.
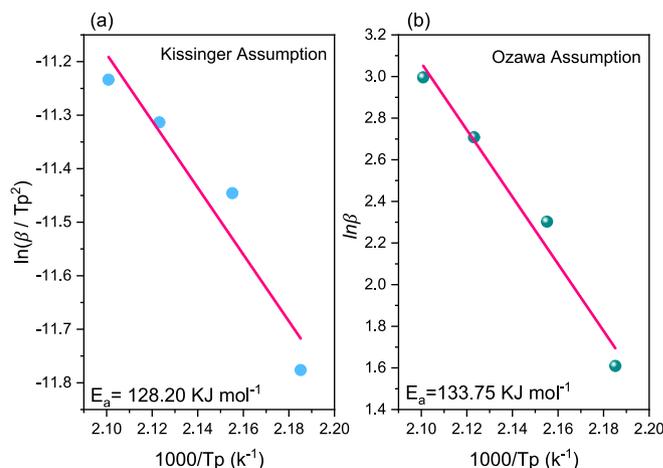

Fig. 4. Activation Energy was calculated from Kissinger (a) and Ozawa (b) assumptions based on the DSC scans of the BGu-BZ.

kinetics and provides a single activation energy value based on peak temperatures. In contrast, the Ozawa method also calculates activation energy but is not limited to linear heating assumptions and can accommodate non-first-order kinetics. In this approach, a plot of ln(β) against T_p^{-1} is used to derive E_a from the slope. The similar values obtained from both methods indicate that the thermal polymerization process exhibits consistent kinetic behavior across different heating rates, enhancing the reliability of these results. The calculated activation energies suggest that the polymerization of BGu-BZ requires significant energy input to initiate and sustain the reaction. These high E_a values reflect the inherent stability of benzoxazine monomers and their resistance to polymerization under mild thermal conditions. Consistent with the Kissinger and Ozawa models, the systematic shift in exothermic peak temperatures with increased heating rates reflects the inherent thermal stability and activation energy of BGu-BZ (128.20 kJ/mol and 133.75 kJ/mol, respectively), distinguishing it from previously reported low-k polybenzoxazine systems that rely on nanofiller reinforcement or complex processing methods for thermal stability and optical functionality [47–49]. The TGA analysis of the uncured BGu-BZ monomer and its cured counterparts at various temperatures (120, 150, 180, and 220 °C) (Fig. 5) provides critical insights into the material's thermal stability and char-forming characteristics. The char yield progressively increases with curing temperature, starting from 41.68 wt% for the BGu-BZ and rising to 42.01 %, 43.59 %, 42.87 %, and 44.95 % for the samples cured at 120 °C, 150 °C, 180 °C, and 220 °C, respectively. This trend indicates that higher curing temperatures enhance cross-linking density within the polymer network, leading to improved thermal stability and greater residual char upon decomposition. Additionally, the T_{d10} values (temperatures at which 10 % mass loss occurs) show significant improvements in thermal stability with curing. The T_{d10} of the uncured monomer is 286.78°C, which increases to 337.79 °C, 369.35 °C, 369.36 °C, and 381.5 °C for samples cured at 120 °C, 150 °C, 180 °C, and 220 °C, respectively. The increase in T_{d10} highlights the effectiveness of the curing process in strengthening the polymer network, enabling it to withstand higher temperatures before substantial degradation.

To analyze the relative chemical composition and electronic states of carbon, nitrogen, oxygen, and bromine in poly(BGu-BZ), XPS measurements were conducted, as shown in Fig. 6. The high-resolution XPS spectra for C 1 s, N 1 s, O 1 s, and Br 3d are presented in Fig. 6(a)-6(d). The C 1 s spectrum of poly(BGu-BZ) was deconvoluted into four distinct peaks (Fig. 6(a)), representing four carbon states: sp² carbons associated with C = C bonds at 284.35 eV, sp² carbons bonded to nitrogen atoms (C-N) at 285.25 eV, carbon atoms bonded to oxygen (C–O) at 285.95 eV, and π-π* transition at 288.00 eV. These findings reveal the complex carbon environment within the polymer matrix. In the N 1 s spectrum (Fig. 6(b)), two nitrogen states were identified at 399.68 eV and 398.63 eV.

These peaks correspond to nitrogen atoms in the triazine ring (N-N) and sp²-nitrogen atoms bonded to two carbon atoms (N-C), respectively, highlighting the diversity of nitrogen environments in the polymer structure. The O1s spectrum (Fig. 6(c)) showed two distinct oxygen states at 535.14 eV and 531.55 eV, attributed to oxygenated species present on the surface (e.g., Na KLL) and oxygen atoms forming bonds with carbon atoms (–CO). This analysis provides insight into the interactions between oxygen and other elements within poly(BGu-BZ). The Br3d spectrum (Fig. 6(d)) revealed two significant peaks at 69.80 eV and 68.29 eV, corresponding to Br-C bonds and Br anions, respectively. These results suggest that bromine contributes to the chemical structure of the polymer, enriching its compositional complexity. A summary of all fitting parameters for the analyzed elements is provided in **Table S1**. This detailed XPS analysis enhances our understanding of the chemical structure and element-specific interactions in poly(BGu-BZ). The porosity characteristics of poly(BGu-BZ) were evaluated through a nitrogen sorption experiment conducted at 77 K [Fig. 7(a) and 7(b)]. The results showed a proportional increase in nitrogen adsorption with rising P/P₀, consistent with a type II isotherm. The initial adsorption rise suggests micropore filling, followed by monolayer formation and subsequent multilayer adsorption as the pressure increases. This behavior indicates that poly(BGu-BZ) likely exhibits microporous characteristics, facilitating significant nitrogen uptake at higher pressures due to capillary condensation. From the adsorption curve (Fig. 7(a)), the Brunauer–Emmett–Teller (BET) specific surface area and pore volume of poly(BGu-BZ)were calculated to be 43 m²/g and 0.081 cm³/g, respectively. Further analysis using nonlocal density functional theory (NLDFT) revealed a pore size distribution with a significant peak at 1.99 nm, indicative of micropores and a mesoporous structure. Additional peaks at 5.29 nm and 9.64 nm (Fig. 7(b)) suggest either particle aggregation or the presence of mesopores within the cured polymer framework. Realistically, these microporous and mesoporous structures of poly(BGu-BZ) enable efficient molecular interactions, which is beneficial for catalysis, sensors, and adsorption-based applications. The structural and morphological properties of poly(BGu-BZ) were further examined using transmission electron microscopy (TEM), providing critical insights into its organization. TEM images [Fig. 7(c) and 7(d)] revealed a self-assembly process that resulted in the formation of uniform micrometer-scale spheres. Statistical analysis of the images determined that the spheres have an average diameter of approximately 18.7 nm. This spherical morphology can be attributed to the guanidinium units within the polymer matrix, which enhance rigidity and promote effective cross-linking. Realistically, the SEM image of the poly(BGu-BZ) proved its spherical morphology [**Fig. S9**]. Further, the elemental SEM-EDS images [Fig. 7(e-h)] confirmed the presence of C, N, O, and Br atoms within the poly(BGu-BZ) structure.

4. The fluorescent properties of BGu-BZ and poly(BGu-BZ)

The synthesis of BGu-BZ, using Gu-3NH₂ and 4-bromo-2-hydroxybenzaldehyde, results in materials with notable solubility characteristics. The uncured BGu-BZ exhibits excellent solubility in various solvents, including DO, tetrahydrofuran (THF), acetone, N,N-dimethylformamide (DMF), and methanol (MeOH). This solubility arises from the structural features of the BGu-BZ. The aromatic bromobenzene ring contributes to stability and favorable electronic properties, allowing effective dissolution in both polar and non-polar solvents [50,51]. Additionally, functional groups such as NH and bromo substituents facilitate hydrogen bonding and dipole–dipole interactions, further enhancing solubility across diverse solvent environments. After
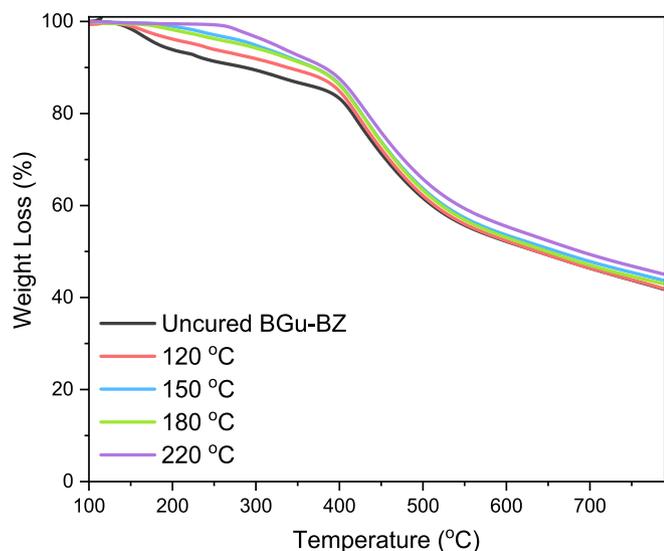

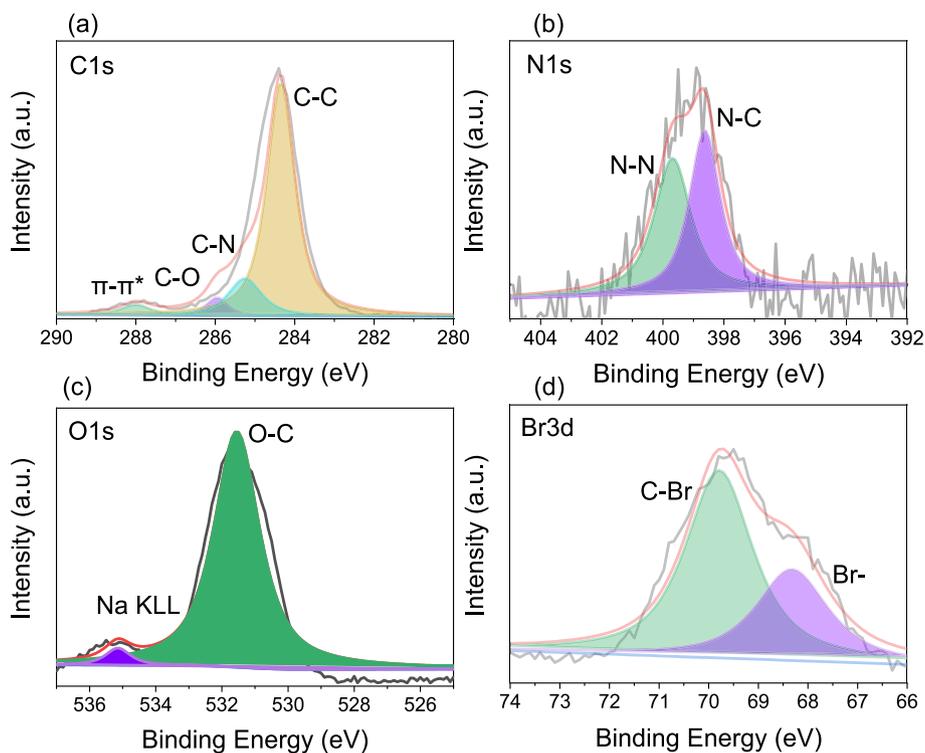**Fig. 5.** TGA analysis of BGu-BZ before and after thermal curing at various temperatures.

Fig. 6. HRXPS of C1s (a), N1s (b), O1s (c), and Br3d (d) of BGu-BZ cured at 220 °C.
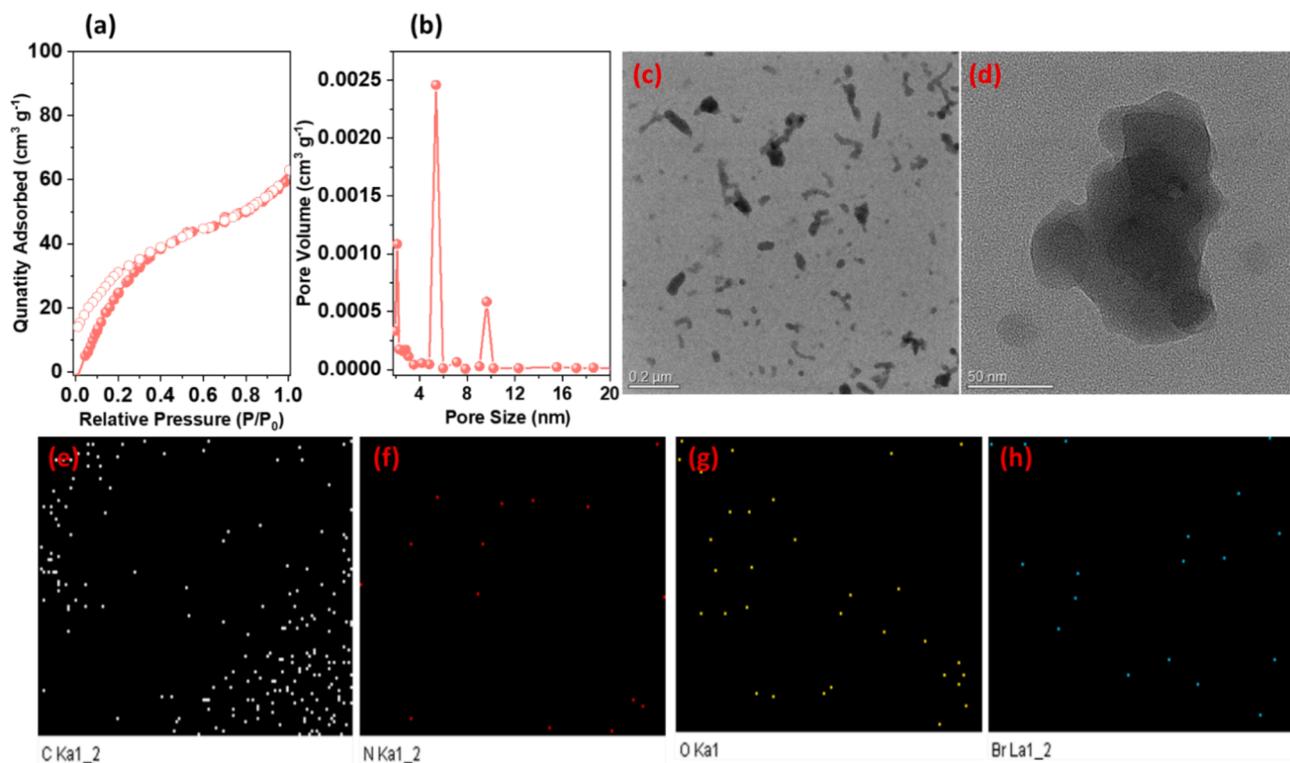

Fig. 7. (a) N$_2$ adsorption isotherm, (b) pore size distribution, (c and d) TEM images at various scales, and (e-h) the elemental SEM-EDS images of poly(BGu-BZ).

curing temperatures ranging from 120 °C to 220 °C, the resulting poly (BGu-BZ) demonstrates good dispersity in the same solvents. The curing process involves cross-linking reactions that enhance the polymer network's rigidity while retaining functional groups capable of interacting with solvent molecules.[52,53] These interactions, such as hydrogen bonding and other intermolecular forces, enable the cured

polymer to maintain favorable dispersity in a variety of solvents. Cross-linking also improves the material's thermal stability and mechanical properties, ensuring robust performance. The UV–vis spectra of BGu-BZ, both before and after curing at 120 °C, 150 °C, and 180 °C [Fig. 8(a)], provide valuable insights into the electronic transitions and structural changes within the material. Absorbance bands observed at 339, 337,
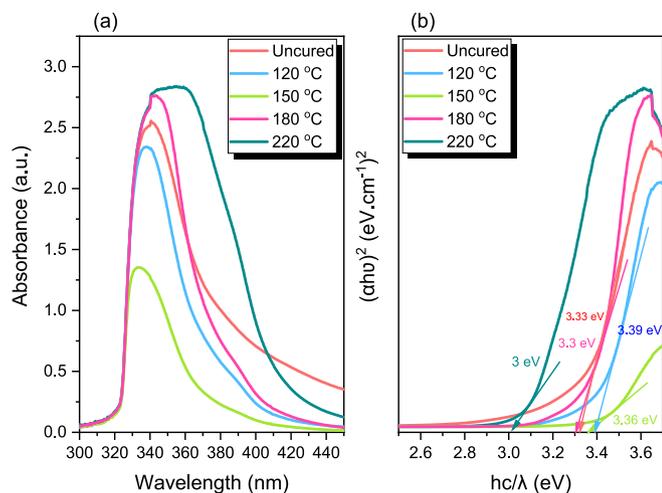
Fig. 8. UV profiles (a) and Tauc plots (b) of BGu-BZ which cured at various series of temperatures (25–220 °C).

336, 341, and 342 nm are indicative of π-π* transitions, characteristic of conjugated aromatic systems. These transitions result from the excitation of electrons from a bonding π orbital to an antibonding π* orbital, highly influenced by the molecular structure and surrounding environment. Before curing, BGu-BZ exhibits distinct absorption peaks, suggesting a well-defined electronic structure. Slight variations in absorbance wavelengths may reflect changes in the local environment around the chromophores, influenced by solvent interactions or conformational flexibility. The presence of closely spaced peaks indicates accessible electronic states, potentially due to variations in hydrogen bonding or solvent interactions. Upon curing at elevated temperatures, structural changes occur in BGu-BZ, resulting in the formation of poly(BGu-BZ). The curing process, involving cross-linking, modifies the electronic environment around chromophores, leading to subtle shifts in absorption peaks or changes in intensity. However, the fundamental electronic transitions remain largely intact, as indicated by the consistent absorbance characteristics across different curing temperatures. This stability highlights the polymer's ability to retain its optical properties despite increased rigidity and reduced chain mobility, which is crucial for applications requiring consistent optical performance. The optical band gap (E_g) of BGu-BZ, both before and after curing, as well as of poly(BGu-BZ), was analyzed using the Tauc–Davis–Mott relationship:

$$(\alpha h\nu)^2 = K(hc/\lambda - E_g).$$

where α is the absorption coefficient, K is a constant, and hc/λ represents the photon energy. The band gap was estimated by plotting $(\alpha hc/\lambda)^2$ against the photon energy hc/λ [54]. This analysis provides insights into the electronic properties of the material, showing how the band gap evolves during the curing process and confirming the stability of the polymer's electronic structure after cross-linking. These findings are crucial for tailoring poly(BGu-BZ) for advanced applications requiring stable optical and electronic properties. The calculated band gaps for BGu-BZ and poly(BGu-BZ) reflect the impact of thermal treatment on the material's electronic structure [Fig. 8(b)]. The band gap of BGu-BZ before curing is 3.33 eV, which increases slightly after curing at 120 °C (3.36 eV) and 150 °C (3.39 eV), then decreases to 3.30 eV at 180 °C, and drops significantly to 3.00 eV for poly(BGu-BZ). These variations highlight how thermal curing influences the polymer's electronic properties. The initial increase in band gap up to 150 °C suggests that curing enhances the rigidity and order of the polymer network. This increased structural order can lead to a more defined electronic state distribution, reducing non-radiative recombination pathways. Consequently, more energy is required for electron excitation, resulting in a higher band gap. At 180 °C, the slight decrease in band gap to 3.30 eV

may indicate structural rearrangements or the onset of chain scission, which can affect electronic properties. Additionally, increased cross-linking density at this temperature might introduce localized states within the band gap, facilitating easier electron transitions [55]. The most significant drop in the band gap to 3.00 eV for poly(BGu-BZ) suggests that extensive curing results in a more complex polymeric structure. This reduction in band gap could be attributed to increased conjugation or delocalization of π-electrons across the polymer backbone [56]. Such changes indicate a transition from localized electronic states in the monomer to a delocalized electronic structure in the polymer, which is a hallmark of many conjugated systems.

These findings provide valuable insights into the evolution of electronic properties during the polymerization process, demonstrating the tunability of poly(BGu-BZ) for applications requiring specific electronic characteristics. The fluorescence emission maxima of BGu-BZ solutions in DO, THF, acetone, DMF, and MeOH were observed at 504, 508, 509, 512, and 501 nm respectively [Fig. 9(a)]. These results demonstrate that the uncured monomer exhibits a relatively consistent emission profile across various solvents, with slight shifts likely influenced by differences in solvent polarity and hydrogen bonding capabilities. The bluish-cyan or blue fluorescence visible to the naked eye suggests that the electronic transitions within the BGu-BZ molecule are predominantly governed by its inherent molecular structure, modulated by the solvent's ability to stabilize its excited states. In polar solvents such as DMF and MeOH, the higher dielectric constant more effectively stabilizes the charged or polar excited states of BGu-BZ compared to less polar solvents like dioxane or THF [57]. This stabilization alters the energy levels associated with the excited states, leading to shifts in emission wavelengths [58]. Conversely, the slight blue shifts observed in less polar solvents may result from reduced stabilization of the excited states, causing emissions to occur at higher energy levels. These findings highlight the interplay between the solvent environment and the photophysical properties of BGu-BZ, emphasizing its potential for tailored fluorescence-based applications. The fluorescence spectra of poly(BGu-BZ) dispersed in the same series of solvents exhibit emission maxima at 413, 507, 543, 560, and 450 nm [Fig. 9(b)]. Compared to the uncured monomer, the significant shift to lower-energy emissions (e.g., 413 nm) highlights a substantial alteration in the electronic structure resulting from the curing process. This transformation is likely due to increased conjugation and rigidity within the polymer matrix, which enables different electronic transitions. The broader range of emission maxima in poly(BGu-BZ) suggests that curing introduces new electronic states or modifies existing ones through cross-linking and structural rearrangements. Longer-wavelength emissions, for example, can be attributed to
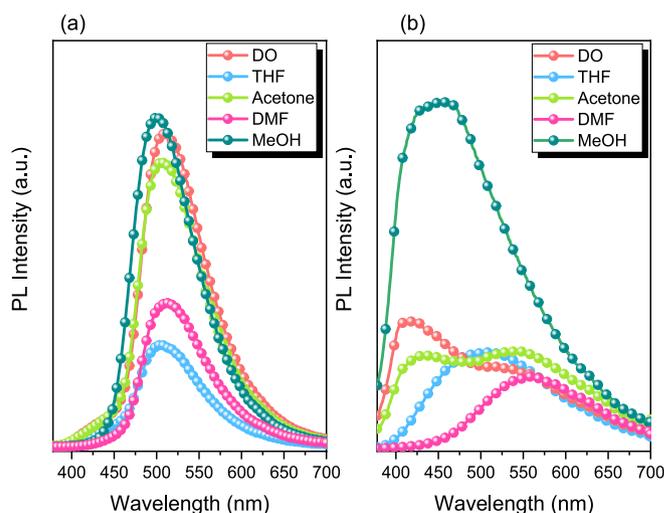

Fig. 9. PL scans of pristine BGu-BZ monomer (a) and poly(BGu-BZ) (b) in various solvents [DO, THF, acetone, DMF, and MeOH; respectively].

the formation of excimers or other aggregate states, phenomena more prevalent in the polymeric environment than in the monomeric state [59–64]. Excimers arise when two fluorophores interact in their excited state, producing unique emission characteristics distinct from those of individual monomers. The solvent-dependent fluorescence properties of BGu-BZ and poly(BGu-BZ) make them excellent candidates for use as solvent sensors. Their distinct fluorescence emission shifts in different solvents allow for precise identification of solvent polarity and composition in chemical processes, quality control, and industrial monitoring. For example, the solvatochromic behavior enables these materials to act as probes for detecting changes in the polarity of their environment. This property can be utilized in studying microenvironments in biological systems, polymer matrices, or complex chemical reactions.

5. Conclusions

This study successfully demonstrated the design, synthesis, and characterization of a novel guanidine-functionalized benzoxazine monomer (BGu-BZ) and its derived porous polymer (poly(BGu-BZ)). The thermal curing process resulted in a highly stable polymer with excellent thermal properties ($T_{d10} = 381.5\,°C$), a moderate surface area ($43\,m^2/g$), and distinct fluorescence shifts due to enhanced conjugation. The solvatochromism behavior of both the monomer and polymer underscores their sensitivity to environmental polarity, making them promising candidates for sensing and optoelectronic applications. The unique combination of porosity, fluorescence, and thermal stability in poly(BGu-BZ) opens up a broad range of practical applications, including solvent sensing, environmental monitoring, and luminescent devices. Furthermore, the scalability and simplicity of the thermal curing process enhance the material's potential for commercial adoption. Future research could explore the functionalization of these materials with other active groups to further enhance their properties, such as increasing surface area for gas adsorption or tailoring fluorescence for specific detection targets. The incorporation of these polymers into composites or devices may also lead to breakthroughs in smart materials and advanced technologies.

CRediT authorship contribution statement

Mohammed G. Kotp: Writing – review & editing, Writing – original draft, Visualization, Investigation, Data curation, Formal analysis, Conceptulatization. **Mohamed Gamal Mohamed:** Writing – review & editing, Writing – original draft, Supervision, Formal analysis, Data curation, Conceptualization. **Aya Osama Mousa:** Writing – original draft, Investigation, Data curation, Formal analysis, Conceptualization. **Shiao-Wei Kuo:** Supervision, Resources, Project administration.

Declaration of competing interest

The authors declare that they have no known competing financial interests or personal relationships that could have appeared to influence the work reported in this paper.

Acknowledgements

Appendix A. Supplementary data

Supplementary data to this article can be found online at https://doi.org/10.1016/j.eurpolymj.2025.113786.

Data availability

The data that has been used is confidential.

References

[1] B. Kiskan, Adapting benzoxazine chemistry for unconventional applications, React. Funct. Polym. 129 (2018) 76–88.
[2] I. Tiwari, P. Sharma, L. Nebhani, Polybenzoxazine-an enticing precursor for engineering heteroatom-doped porous carbon materials with applications beyond energy, environment and catalysis, Mater. Today Chem. 23 (2022) 100734.
[3] S. Mukherjee, N. Amarnath, B. Lochab, Oxazine ring-substituted 4th generation benzoxazine monomers & polymers: stereoelectronic effect of phenyl substituents on thermal properties, Macromolecules 54 (2021) 10001–10016.
[4] N. Ghosh, B. Kiskan, Y. Yagci, Polybenzoxazines—new high performance thermosetting resins: synthesis and properties, Prog. Polym. Sci. 32 (2007) 1344–1391.
[5] I. Machado, I. Hsieh, E. Rachita, M.L. Salum, D. Iguchi, N. Pogharian, A. Pellot, P. Froimowicz, V. Calado, H. Ishida, A truly bio-based benzoxazine derived from three natural reactants obtained under environmentally friendly conditions and its polymer properties, Green Chem. 23 (2021) 4051–4064.
[6] E.I. Bîru, S.A. Gârea, H. Iovu, Developing polybenzoxazine composites based on various carbon structures, Macromol. Chem. Phys. 220 (2019) 1800322.
[7] V. Vatanpour, B. Kiskan, B. Zeytuncu, I. Koyuncu, Polybenzoxazines in fabrication of separation membranes: A review, Sep. Purif. Technol. 278 (2021) 119562.
[8] J. Liu, N. Safronova, R.E. Lyon, J. Maia, H. Ishida, Enhanced thermal property and flame retardancy via intramolecular 5-membered ring hydrogen bond-forming amide functional benzoxazine resins, Macromolecules 51 (2018) 9982–9991.
[9] S. Mukherjee, B. Lochab, Hydrogen bonding-guided strategies for thermal performance modulation in biobased oxazine ring-substituted benzoxazine thermosets, Macromolecules 57 (2024) 1795–1807.
[10] Y.C. Kao, Y.H. Ku, M.G. Mohamed, W.H. Su, S.W. Kuo, Microphase Separation Transformation in Bio-Based Benzoxazine/Phenolic/PEO-b-PCL Diblock Copolymer Mixtures Induced by Transesterification Reaction, Macromolecules 58 (2025) 585–600.
[11] M. Ejaz, M.G. Mohamed, W.C. Huang, Y.C. Kao, W.C. Chen, S.W. Kuo, Highly thermally stable polyhedral oligomeric silsesquioxane based on diacetal-functionalized polybenzoxazine nanocomposites, Eur. Polym. J. 223 (2025) 113649.
[12] C.J. Higginson, K.G. Malollari, Y. Xu, A.V. Kelleghan, N.G. Ricapito, P. B. Messersmith, Bioinspired design provides high-strength benzoxazine structural adhesives, Angew. Chem. Int. Ed. 131 (2019) 12399–12407.
[13] M.G. Mohamed, S.W. Kuo, Functional Silica and Carbon Nanocomposites Based on Polybenzoxazines, Macromol. Chem. Phy. 220 (2019) 1800306.
[14] M.M. Samy, M.G. Mohamed, S.W. Kuo, Pyrene-functionalized tetraphenylethylene polybenzoxazine for dispersing single-walled carbon nanotubes and energy storage, Compos. Sci. Technol. 199 (2020) 108360.
[15] J. Song, H. Liang, Y. Cao, M. Wang, Z. Wang, Advancing Coatings with Polybenzoxazines: Insights into Molecular Design, Synthesis, and Modification, J. Mater. Chem. C 12 (2024) 9094–9111.
[16] K.I. Aly, M.G. Mohamed, O. Younis, M.H. Mahross, M. Abdel-Hakim, M.m., Sayed, Salicylaldehyde azine-functionalized polybenzoxazine: Synthesis, characterization, and its nanocomposites as coatings for inhibiting the mild steel corrosion, Prog. Org. Coat. 138 (2020) 105385.
[17] K. Mohamed Mydeen, B. Krishnasamy, H. Arumugam, A. Muthukaruppan, Eco-friendly bio-based polybenzoxazine composites derived from sustainable thymol: A versatile approach and multifaceted study for enhanced applications, J. Polym. Sci. 62 (2024) 3959–3978.
[18] S. Minkovska, G.B. Hadjichristov, A. Neacsu, V. Chihaia, Y.V. Fedorov, Photoswitchable Photochromic Chelating Spironaphthoxazines: Synthesis, Photophysical Properties, Quantum-Chemical Calculations, and Complexation Ability, ACS Omega 9 (2024) 4144–4161.
[19] X.-L. Sha, L. Yuan, G. Liang, A. Gu, Preparation of high performance bio-based benzoxazine resin through a green solvent-free strategy for shape memory application, Polymer 202 (2020) 122673.
[20] K.I. Aly, S.M. Ebrahium, H.N. Abdelhamid, H.M. El-Bery, A.A.K. Mohammed, C. W. Huang, M.G. Mohamed, Efficient synthesis of main chain thermosetting polybenzoxazine resin containing tert-butylcyclohexanone and diphenylmethane units for supercapacitor energy storage, Eur. Polym. J. 221 (2024) 113519.
[21] S. Gulyuz, B. Kiskan, Combining Siloxane-Based polybenzoxazine with Poly (ethylene-co-vinyl acetate/hydroxyl) for tougher, more Stable, and Self-Healable materials, Eur. Polym. J. 212 (2024) 113073.
[22] S. Leungpuangkaew, L. Amornkitbamrung, N. Phetnoi, C. Sapcharoenkun, C. Jubsilp, S. Ekgasit, S. Rimdusit, Magnetic-and light-responsive shape memory polymer nanocomposites from bio-based benzoxazine resin and iron oxide nanoparticles, Adv. Ind. Eng. Polym. Res. 6 (2023) 215–225.
[23] Y. Liang, M. Xia, Q. Yu, Y. Li, Z. Sui, Y. Yuan, X.-M. Hu, Q. Chen, N. Wang, Guanidinium-based ionic covalent organic frameworks for capture of uranyl tricarbonate, Adv. Compos. Mater. 5 (2022) 184–194.
[24] H. Tang, Y. Kang, S. Cao, Z. Chen, Synthesis and performance of guanidinium-based cationic organic polymer for the efficient removal of TcO4-/ReO4-, J. Hazard. Mater. 466 (2024) 133602.
[25] D. Plaul, M. Böhme, S. Ostrovsky, Z. Tomkowicz, H. Görls, W. Haase, W. Plass, Modeling spin interactions in a triangular cobalt (II) complex with

triaminoguanidine ligand framework: synthesis, structure, and magnetic properties, Inorg. Chem. 57 (2018) 106–119.

[26] X.-X. Zhang, Z.-H. Xue, J.-L. Hao, W. Qiao, Q.-L. Yan, Structural Control of Energetic Triaminoguanidine Nitrate Polymer Nanostructures for Reduced Thermal Reactivity, ACS Appl. Nano Mater. 6 (2023) 17890–17901.

[27] W. Zhou, Y. Wang, F. Kong, W. Peng, Y. Wang, M. Yuan, X. Han, X. Liu, B. Li, Advances in liquid crystal epoxy: molecular structures, thermal conductivity, and promising applications in thermal management, Energy Environ. Mater. 7 (2024) e12698.

[28] S. Kohúteková, I. Matulková, M. Zábranský, J.L. Martín, I. Císařová, R. Gyepes, P. Němec, M. Gryl, T. Seidler, I. Němec, New group of inorganic salts of 1, 3-dia-minoguanidinium (1+) cation–crystal structures, vibrational spectra, linear and nonlinear optical properties, J. Solid State Chem. 327 (2023) 124288.

[29] W. Shi, X. Zhao, S. Ren, W. Li, Q. Zhang, X. Jia, Heteroatoms co-doped porous carbons from amino acid based polybenzoxazine for superior CO_2 adsorption and electrochemical performances, Eur. Polym. J. 165 (2022) 110988.

[30] X. Yuan, L. Liu, Y. Wang, Q. Jiang, Y. Shi, G. Wang, Tyrosine-based branched polybenzoxazines with antibacterial and surface fouling released performances for marine antifouling coatings, Prog. Org. Coat. 200 (2025) 108978.

[31] Y. Miyagi, M. Goto, M. Minami, F. Sanda, Synthesis and Properties of Amino Acid-based Optically ActivePoly (benzoxazine)s, J. Adhes. Soc. Jpn. 53 (2017) 338–347.

[32] S. Mitra, S. Kandambeth, B.P. Biswal, A. Khayum M, C.K. Choudhury, M. Mehta, G. Kaur, S. Banerjee, A. Prabhune, S. Verma, Self-exfoliated guanidinium-based ionic covalent organic nanosheets (iCONs), J. Am. Chem. Soc., 138 (2016) 2823-2828.

[33] A. Hassan, S. Chandra, A. Alam, N. Das, Super-fast iodine capture by an ionic covalent organic network (iCON) from aqueous and vapor media, RSC Sustain. 1 (2023) 511–522.

[34] M.G. Mohamed, W.-C. Chang, S.-W. Kuo, Crown ether-and benzoxazine-linked porous organic polymers displaying enhanced metal ion and CO_2 capture through solid-state chemical transformation, Macromolecules 55 (2022) 7879–7892.

[35] M.G. Mohamed, C.-J. Li, M.A.R. Khan, C.-C. Liaw, K. Zhang, S.-W. Kuo, Formaldehyde-free synthesis of fully bio-based multifunctional bisbenzoxazine resins from natural renewable starting materials, Macromolecules 55 (2022) 3106–3115.

[36] M.M. Samy, M.G. Mohamed, T.H. Mansoure, T.S. Meng, M.A.R. Khan, C.-C. Liaw, S.-W. Kuo, Solid state chemical transformations through ring-opening polymerization of ferrocene-based conjugated microporous polymers in host–guest complexes with benzoxazine-linked cyclodextrin, J. Taiwan. Inst. Chem. Eng. 132 (2021) 104110, https://doi.org/10.1016/j.jtice.2021.10.010.

[37] M.G. Mohamed, B.-X. Su, S.-W. Kuo, Robust nitrogen-doped microporous carbon via crown ether-functionalized benzoxazine-linked porous organic polymers for enhanced CO_2 adsorption and supercapacitor applications, ACS Appl. Mater. Interfaces 16 (2024) 40858–40872.

[38] M. Ejaz, M.G. Mohamed, S.-W. Kuo, Fluorescent benzoxazine–perylene linked covalent organic polymer as a sensing probe for lead ions and 2,4,6-trinitrophenol, ACS Appl. Polym. Mater. 6 (2024) 9170–9179.

[39] M. Ejaz, M.G. Mohamed, Y.-T. Chen, K. Zhang, S.-W. Kuo, Porous carbon materials augmented with heteroatoms derived from hyperbranched biobase benzoxazine resins for enhanced CO_2 adsorption and exceptional supercapacitor Performance, J Energy Storage 78 (2024) 110166.

[40] Y. Lu, N. Li, Y. Peng, M.G. Mohamed, S.-W. Kuo, K. Zhang, Facile and eco-friendly synthesis of hydrogen bonding-rich bio-based bisbenzoxazine resins with low surface free energy, strong adhesion strength and high thermal stability, Mol. Syst. Des. Eng. 9 (2024) 86–98.

[41] C.Y. Chen, W.C. Chen, M.G. Mohamed, Z.Y. Chen, S.W. Kuo, Highly Thermally Stable, Reversible, and Flexible Main Chain Type Benzoxazine Hybrid Incorporating Both Polydimethylsiloxane and Double-Decker Shaped Polyhedral Silsesquioxane Units through Diels–Alder Reaction, Macromol. Rapid Commun. 44 (2023) 2200910.

[42] Z.-Y. Chen, W.-C. Chen, S.-W. Kuo, Enhanced thermal and porous properties of double-decker-shaped polyhedral silsesquioxane-bismaleimide (DDSQ-BMI) nanocomposites for high-performance CO_2 storage and supercapacitors, Polym. Chem. 15 (2024) 553–564.

[43] S. Vyazovkin, D. Achilias, X. Fernandez-Francos, A. Galukhin, N. Sbirrazzuoli, ICTAC Kinetics Committee recommendations for analysis of thermal polymerization kinetics, Thermochim. Acta 714 (2022) 179243.

[44] J. Wang, X. Fang, M.-Q. Wu, X.-Y. He, W.-B. Liu, Synthesis, curing kinetics and thermal properties of bisphenol-AP-based benzoxazine, Eur. Polym. J. 47 (2011) 2158–2168.

[45] J.J. Benvenuta-Tapia, E. Vivaldo-Lima, J.A. Tenorio-López, M. de los Ángeles Vargas-Hernández, H. Vázquez-Torres, Kinetic analysis of the RAFT copolymerization of styrene and maleic anhydride by differential scanning calorimetry, Thermochim. Acta, 667 (2018) 93-101.

[46] J. Orava, A. Greer, Kissinger method applied to the crystallization of glass-forming liquids: regimes revealed by ultra-fast-heating calorimetry, Thermochim. Acta 603 (2015) 63–68.

[47] A. Amalorpavadoss, S. Kumar, V. Pavunkumar, A. Chandramohan, K. Dinakaran, G. Harichandran, Synthesis, Characterization and anti-corrosion property of GPTMS functionalized mesoporous silica (F-SBA-15) incorporated aliphatic chain containing polybenzoxazine nanocomposites, Compos, Interfaces 29 (2022) 833–852.

[48] S. Kumar, A. Hariharan, A. Muthukaruppan, D. Roy, K. Dinakaran, Synthesis and characterization of graphene oxide reinforced triphenyl pyridine-based polyimide composites having UV shielding and low k properties, Compos, Interfaces 29 (2022) 37–55.

[49] S. Kumar, H. Arumugham, D. Roy, D. Kannaiyan, Synthesis and characterization of fluorine functionalized graphene oxide dispersed quinoline-based polyimide composites having low-k and UV shielding properties, Polym. Adv. Technol. 33 (2022) 427–439.

[50] T.M. Krygowski, M.K. Cyrański, Structural aspects of aromaticity, Chem. Rev. 101 (2001) 1385–1420.

[51] Z. Zeng, X. Shi, C. Chi, J.T.L. Navarrete, J. Casado, J. Wu, Pro-aromatic and anti-aromatic π-conjugated molecules: an irresistible wish to be diradicals, Chem. Soc. Rev. 44 (2015) 6578–6596.

[52] J.W. Stansbury, Dimethacrylate network formation and polymer property evolution as determined by the selection of monomers and curing conditions, Dent. Mater. 28 (2012) 13–22.

[53] P. Song, H. Wang, High-performance polymeric materials through hydrogen-bond cross-linking, Adv. Mater. 32 (2020) 1901244.

[54] S.U. Sharma, M.H. Elsayed, I.M.A. Mekhemer, T.S. Meng, H.H. Chou, S.W. Kuo, M. G. Mohamed, Rational design of pyrene and thienyltriazine-based conjugated microporous polymers for high-performance energy storage and visible-light photocatalytic hydrogen evolution from water, Giant 17 (2024) 100217.

[55] S. Chu, Y. Wang, Y. Guo, J. Feng, C. Wang, W. Luo, X. Fan, Z. Zou, Band structure engineering of carbon nitride: in search of a polymer photocatalyst with high photooxidation property, ACS Catal. 3 (2013) 912–919.

[56] L. Dou, Y. Liu, Z. Hong, G. Li, Y. Yang, Low-bandgap near-IR conjugated polymers/molecules for organic electronics, Chem. Rev. 115 (2015) 12633–12665.

[57] İ. Sıdır, Y.G. Sıdır, H. Berber, F. Demiray, Emerging ground and excited state dipole moments and external electric field effect on electronic structure. A solvatochromism and theoretical study on 2-((phenylimino) methyl) phenol derivatives, J. Mol. Liq. 206 (2015) 56–67.

[58] A. Samanta, Dynamic stokes shift and excitation wavelength dependent fluorescence of dipolar molecules in room temperature ionic liquids, J. Phys. Chem. B 110 (2006) 13704–13716.

[59] C.H. Chen, K. Satyanarayana, Y.H. Liu, S.L. Huang, T.S. Lim, T.Y. Luh, Excimer Formation in a Confined Space: Photophysics of Ladderphanes with Tetraarylethylene Linkers, Chem. Eur. J. 21 (2015) 800–807.

[60] M.G. Kotp, S.-W. Kuo, Harnessing solar energy with porous organic polymers: Advancements, challenges, economic, environmental impacts and future prospects in sustainable photocatalysis, Mater. Today Chem. 41 (2024) 102299.

[61] M.G. Kotp, C.-L. Chang, A.F.M. EL-Mahdy, Tetraphenyl-p-phenylenediamine-based tunable conjugated microporous polymers: Adsorption and photodegradation of hazardous dyestuff in aqueous environments, J. Water Process Eng. 53 (2023) 103675.

[62] M.G. Mohamed, K.C. Hsu, J.L. Hong, S.W. Kuo, Unexpected fluorescence from maleimide-containing polyhedral oligomeric silsesquioxanes: nanoparticle and sequence distribution analyses of polystyrene-based alternating copolymers, Polym. Chem. 7 (2016) 135–145.

[63] M.G. Mohamed, F.H. Lu, J.L. Hong, S.W. Kuo, Strong emission of 2,4,6-triphenyl-pyridine-functionalized polytyrosine and hydrogen-bonding interactions with poly (4-vinylpyridine), Polym. Chem. 6 (2015) 6340–6350.

[64] Y. Zheng, P. Chen, Z. Niu, E. Wang, Excimer emission from polycyclic arenes bearing triphenylmethyl group: Solid-state fluorescence, mechanofluorochromism, aggregation-induced emission and cell imaging application, Spectrochim. Acta A Mol. Biomol. Spectrosc. 312 (2024) 124035.